CHARACTERISTICS OF EJECTORS ON SMALL GAS TURBINE ENGINES

J. Georgi, S. Staudacher
Institute of Aircraft Propulsion Systems
University of Stuttgart
Pfaffenwaldring 6, 70569 Stuttgart, Germany

Abstract

Unmanned, scaled flight demonstrators are used to investigate new airplane designs. The demonstrators are generally driven by small jet engines because jet engines are also used for airplanes. Small jet engine designs may include a fan, an aft-fan, a geared fan or an ejector. Ejector design has the advantage of low weight and simplicity.
We examined the characteristics of a small jet engine with ejector, first qualitatively, using a water channel and then quantitatively, using a test rig. The experimental setups and the gathered test data are briefly presented.

NOMENCLATURE

A	Area
F	Force
L	Length
Ma	Mach number
T	Temperature
c	Coefficient
d	Diameter
h	Water height
$\dot{m}$	Mass flow
p	Pressure
v	Velocity
ε	Area ratio
ζ	Velocity ratio
λ	Length ratio
ρ	Density
ϕ	Thrust augmentation

Indices

BPR	Bypass ratio
D	Flow rate
DK	Pressure force
FK	Spring force
G	Gross
N	Net
a	Average
ej	With ejector
f	Flight
id	Ideal
in	Inlet
l	Local
t	Total
0	Ambient
5	Nozzle primar flow entry
60	Ejector primary flow entry / mixing plane
61	Ejector secondary flow entry
9	Ejector exit

1. INTRODUCTION

Unmanned, scaled flight demonstrators are used to examine new airplane configurations. They are driven by small jet engines in the thrust class between 15 and 500 N. They are preferred to propeller drives because of the desired similarity to the original aircraft. Examples for the scaled flight demonstrators are the experimental airplanes in the projects NACRE and VELA2 as described by Nguewo [1]. They should provide insights into the aerodynamic and aero-mechanical properties of the original aircraft. The flight speed of such vehicles is limited by the requirement for similar flight performance. Here Mach numbers up to Ma = 0.2 are achieved.
The resulting ratio between jet and flight speed is not similar to the original aircraft. This results in a jet spreading that differs from the original one and affects the airflow around the wings and the flaps [2]. In order to minimize these differences, small jet engines with a bypass-ratio should be used in scaled flight demonstrators. Feasible designs, such as fan, aft-fan, geared fan, two-shaft turbofan or ejector differ in complexity, power, weight and optimal operating range. The focus of this work lies on the study of ejectors, because they offer the advantages of small weight and low complexity. Moreover, ejectors on small jet engines have not been a subject of scientific investigations. They differ in size and similarity parameters from previous studies.

2. EJECTOR OPERATION

An ejector is a jet pump without moving parts, see Fig. 1. It can be defined by a nozzle of the area A_{60} and of a constant cross-section mixing chamber of the area A_9 and length L. Shear forces between the primary and secondary flow cause a mixing process of both streams and a static pressure drop below ambient pressure in the mixing plane [3] [4]. Energy is transferred between the flows.
The kinetic energy of the primary stream is distributed on a larger mass flow of air. The specific enthalpies of the two streams equalize and the ejector exhaust velocity v_9 decreases. For this reason propulsive efficiency increases. As a result thrust augmentation can be achieved [5]. This

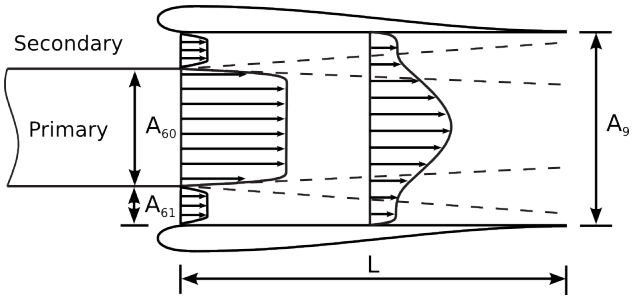

Fig. 1: Geometry, nomenclature, velocity profiles and mixing process between primary and secondary stream in an ejector.

is the ratio of the specific net thrusts with and without ejector. Because the ejector reduces static pressure after the primary nozzle an increase of primary mass flow $\dot{m}_{60,ej}$ is the consequence. Therefore thrust augmentation factor ϕ is defined as

$$\phi = \frac{F_{ej}/\dot{m}_{60,ej}}{F/\dot{m}_{60}}. \quad (1)$$

Thrust augmentation is highly dependent on the operating point of the small jet engine and the ejector geometry. The operating point is defined by the flight Mach number Ma_f, the total temperature ratio $T_{t,60}/T_{t,61}$ and the engine pressure ratio $p_{t,60}/p_{t,0}$. Typical values for small gas turbine engines within this context are $0 \leq Ma_f \leq 0.2$, $2.4 \leq T_{t,60}/T_{t,61} \leq 3$ and $1 \leq p_{t,60}/p_{t,0} \leq 1.9$. The geometry is described by two non-dimensional variables, the area ratio

$$\varepsilon = \frac{A_{60}}{A_{60} + A_{61}} \quad (2)$$

and the length ratio

$$\lambda = \frac{L}{d_{60}}. \quad (3)$$

3. EXPERIMENTAL INVESTIGATIONS

In Fig. 2 experimental investigations on ejectors from the early sixties until today are categorized and plotted in dependance of ε and λ. In this studies investigations on ejectors as jet pumps are excluded because jet pumps are mainly used for incompressible fluids. The ejectors can be classified in the group of thrust augmentation for Vertical/Short Takeoff and Landing (V/STOL) aircrafts [6] and noise suppressors for older airplanes to meet noise regulation requirements. The design of the thrust augmentors was based on ideal conservation equations of mass, energy and momentum and are characterized by small area ratios ε [7] [8] and high length ratios λ [9] [10]. Noise suppressing ejectors are limited by the available installation space of the airplanes and tend to a larger area ratio ε. Later the ejector length was reduced with forced mixing techniques to reduce drag during flight [11] [5]. Ejectors on small jet engines have been only scarcely investigated [12] [13].
Small jet engines are larger than jet pumps and smaller than

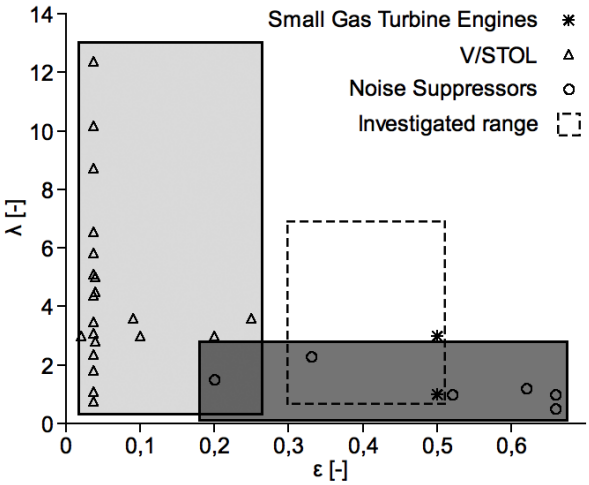

Fig. 2: The optimum performance of ejectors on small jet engines lies between the ranges of V/STOL and noise suppressor applications.

realized aircraft engines. It is expected that the specific geometric relations of ε and λ is important to the aerodynamics and to the ejector performance. Therefore, in the present work a range of $0.3 \leq \varepsilon \leq 0.5$ and $0 < \lambda < 7$ is investigated experimentally, see Fig. 2.
The experimental investigations have been done in two distinctive steps. In the first step water channel experiments have been carried out. The aim was to understand basic flow phenomena. The focus lay on possibly special flow phenomena for the specified ε-λ range. In the second step an ejector test rig has been used. The aim was to quantify ejector performance for small jet engines in the same ε-λ range.

3.1. Water channel

A schematic design of the water channel is shown in Fig. 3. A pump delivers water through a pipe to a reservoir from where it continues through downpipes to the main basin. This arrangement reduces the influence of the fluctuating pump flow rate. For reducing turbulence, the water passes through a combination of sieves and honeycombs. Afterwards, it is accelerated through a nozzle and enters the measuring section which has a length of 120 cm and a width of 30 cm. A camera installed vertically above the measuring section allows the recording of single frames as well as video at a rate of 50 frames per second.
Because water has a higher viscosity than air, no Reynolds number similarity can be achieved in this water channel. To model the ejector as large as possible, it is realized as a half section. A separating plate divides the measuring section into a primary and a secondary part as shown in Fig. 4. Flow conditions in the measuring section is characterized by the velocity ratio

$$\zeta = \frac{v_{60} - v_0}{v_{60} + v_0} \quad (4)$$

which is a number for the speed distribution between the primary and secondary flow. Flow conditions within the measuring section are set by weirs in a way which takes

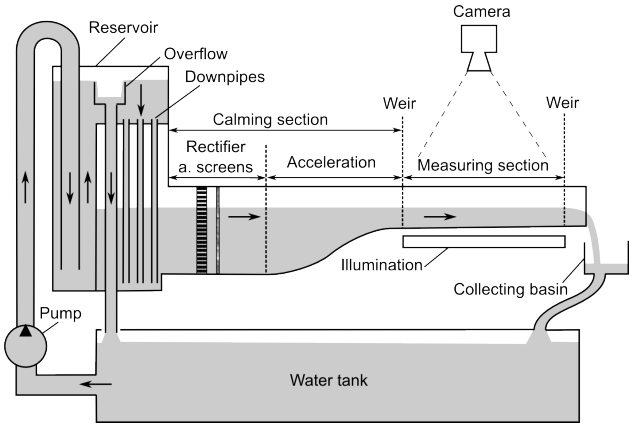

Fig. 3: Schematic design of the water channel.

care that during a series of measurements the overall mass flow and the water height h remain constant. Therefore, for each velocity ratio within a series of measurements the same average flow velocity v_a is given. On this average flow velocity an average Reynolds number

$$Re_a = \frac{v_a h}{\nu}. \quad (5)$$

is established. Under these conditions two measurement series at constant average Reynolds numbers of Re_a = 2770 and 10250 at a constant water height of h = 0.11 m in the measuring section were carried out.

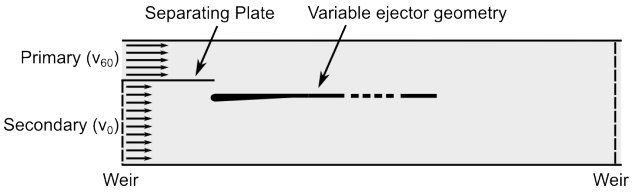

Fig. 4: Measuring section with separating plate, variable ejector geometry and weirs.

The flow around the trailing edge of the separating plate was visualized for two cases: with and without ejector. A diluted ink solution was injected into the boundary layers of the separating plate. The resulting mixing cone can be displayed by superpositioning of frames. The mixing is characterized geometrically by two parameters. The opening angle α describes the spreading of the mixing zone and thus is a measure for the mixing intensity. The deflection angle β is the angle between the bisection of the opening angle and the extension of the separating plate. It describes the deflection of the mixing cone relative to the main flow direction, see Fig. 5. The angles were evaluated by averaging multiple measurements. Gross errors were treated as described in [14].
The opening angles for the case without ejector were measured by Strehblow [15]. The results are compared to data from earlier experimental mixer investigations by Banzhaf [16] at the same water channel with a similar geometric setup, see Fig. 6. For small Re_a and ζ = 0 no mixing occurs. If we increase Re_a, a Karman vortex street is formed and an opening angle can be measured. The frequency of

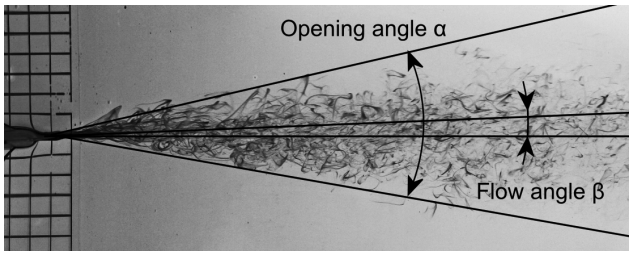

Fig. 5: Superimposing of multiple individual frames and evaluation of opening and deflection angle [15].

the Karman vortex street depends on the thickness of the trailing edge and Re_a. With increasing velocity ratio ζ Kelvin-Helmholtz vortices occur, causing an intense mixing of core and ambient flow. It was observed that for $\zeta > 0.5$ the opening angle α increases linearly as described by Sabin [17]. The Flow angle β indicates a slight deflection towards the faster stream.

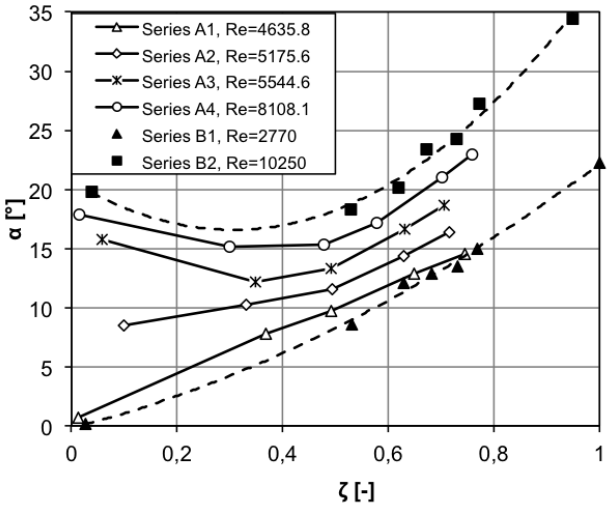

Fig. 6: Comparison of free jet opening angles after a separating plate at different average Reynolds numbers. Series A1-A4 were done by Banzhaf [16].

In further series of experiments at an average Reynolds number of Re_a = 10250 a variable ejector was involved. For the constant length ratio of λ = 1.69 and velocity ratios of ζ = 0.53 and 0.68 the ejector area ratio ε was varied, see Fig. 7. It was observed that opening angles for all measurements are smaller with ejector than without it. Moreover, the opening angles depend on the area ratio. For increasing area ratio the opening angles decrease.
Ahmed [18] mentioned that wall effect is one of the reasons for the decreasing mixing layer growth. Thus an increasing area ratio leads to more confinement of the flow which decreases the opening angles.
Moreover, for constant area ratio and length ratio with increasing velocity ratio the slope of the curves decreases, see Fig. 8. The difference in opening angles between the free jet and within the ejector increases with increasing velocity ratio. This effect can be explained with ejector pumping. Within the ejector a local velocity parameter ζ_l can be formed

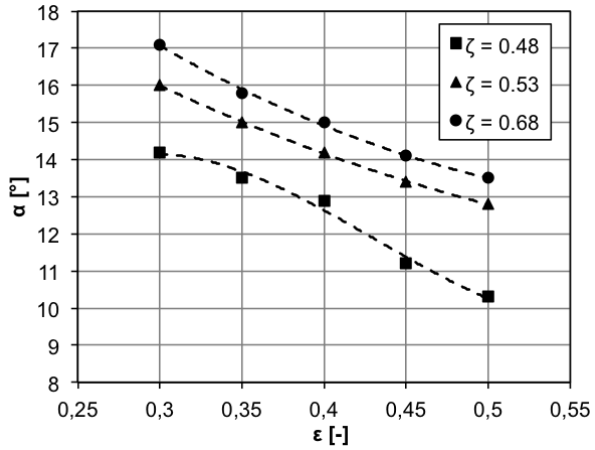

Fig. 7: Opening angle with ejector for λ = 1.69 and Re_a = 10250.

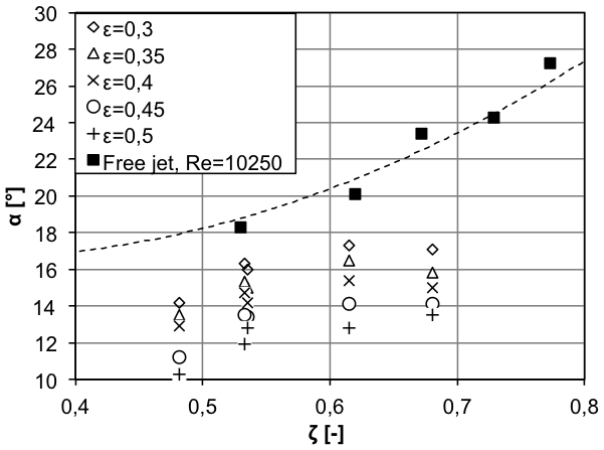

Fig. 8: With increasing velocity ratio the difference between the free jet opening angle and the opening angles with ejector for λ = 1.69 and Re_a = 10250 increases.

with the bypass flow velocity v_{61} in the bypass entry area. Bypass flow velocity v_{61} rises above ambient flow velocity v_0. This causes the local velocity parameter ζ_l to decrease and reduce the mixing intensity of both flows within the ejector. For this reason, ejector pumping was visualized with streamlines in the inlet region of the ejector. Images from multiple experiments were superimposed and compared qualitatively. An example is given in Fig. 9 for the configurations ζ = 0 and ζ = 0.68. For ζ = 0.68 a flow exists around the inlet lip toward the ejector inside. The ejector pumps in fluid causing $v_{61} > v_0$. With decreasing velocity ratio the pumping and thus bypass velocity v_{61} reduces. For ζ = 0 the streamlines are deflected towards the ambient flow. In the flight case, this would cause a loss of thrust.

It was also observed that the ejector length ratio has an influence on opening angle. The reason is mainly the growing boundary layer along the inner wall of the ejector as described by Ginevski [20]. Maintaining a constant area ratio of ε = 0.3 the length ratio λ was varied, see Fig. 10. With increasing length ratio the opening angles decrease. The slight bents in all three curves are caused by the bypass

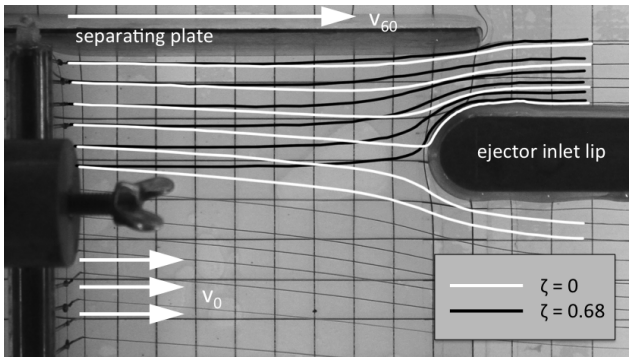

Fig. 9: Flow streamlines for different values of the velocity ratio ζ [19]. Higher values of ζ increase ejector pumping.

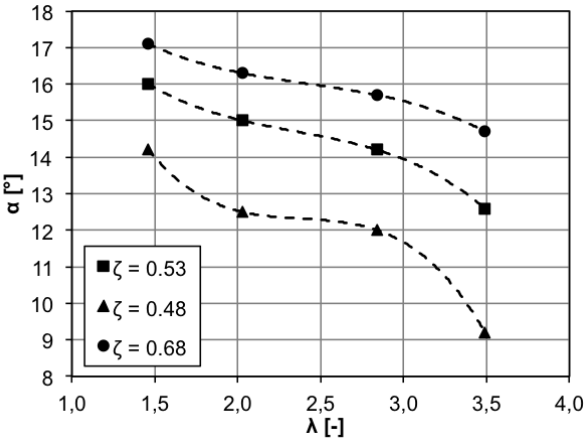

Fig. 10: Opening angle with ejector for ε = 0.3 and Re_a = 10250.

stream which is partially mixed for $\lambda < 3$ and completely mixed for values above.

3.2. Ejector test rig

The effects of the variables ε and λ on the ejector performance shall be quantified at the ejector test rig. The schematic layout of the test rig with nomenclature is shown in Fig. 11. The rig is scaled to match a representative jet engine with a net thrust of 300 N . The pressure of the core flow can be adjusted with the valve L01. The air passes through a rectifier and orifice plate, then flows through an expansion joint which allows axial movement of the measurement slide. It enters the ejector through the primary nozzle 60 and entrains a secondary flow through the area 61. The stream exits the ejector to the ambient in 9.

Because the ejector is of constant diameter, ε can be varied by changing the primary nozzle. The length parameter λ is altered by varying the ejector length using extension tubes. The secondary flow is entrained from stationary air. Therefore only velocity ratios of ζ = 1 can be examined.

The test rig enables measuring of velocity profiles at the ejector outlet, of static pressure along the ejector mixing chamber as well as the thrust with and without ejector, from which the thrust augmentation factor is derived.

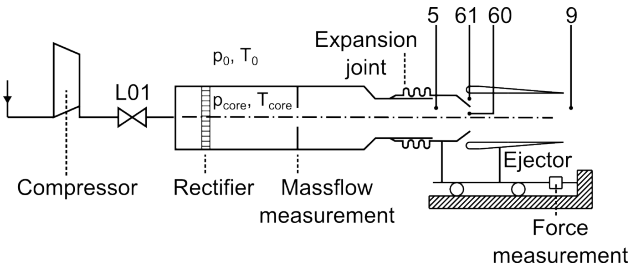

Fig. 11: Overall concept of the ejector test rig. An expansion joint allows axial movement.

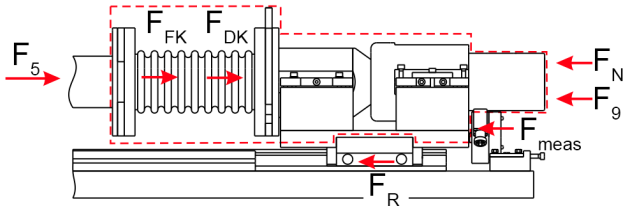

Fig. 12: The net thrust can be determined with a control volume approach around the test rig. The relevant force vectors are indicated [22].

A variation of the average Reynolds number, as it was done at the water channel, can be realized by varying the primary nozzle total pressure $p_{t,60}$. Because Reynolds numbers at water channel and ejector test rig are not comparable the pressure ratio $p_{t,60}/p_{t,0}$ is used instead of Re_a to characterize the different operating conditions.

3.2.1. Measurement technology

Sheathed individually calibrated thermocouples of type K were used on the test bench. The recovery factor was calculated iteratively.
Static pressures were measured at wall holes with a diameter of 0.5 mm along the measurement path. For the measurement of total pressure pitot tubes were used with an outside diameter of 1.0 mm. These pitot tubes require a small installation space and cause a slight obstruction in the flow channel. At the outlet of the ejector, a traversable Prandtl probe was used to measure static and total pressure. The pressure measurement was performed with calibrated measurement modules of different type. Their operating range extends from 5 to 100 PSI.
The core mass flow was measured by an orifice plate with an integrated ring measuring chamber. The measurement setup was built according to the highest accuracy in the DIN EN ISO 5167 Part 2 standard.
A thrust measurement was installed at the measuring slide which can handle forces between 0 and 500 N. The net force F_N of the ejector system can not be measured directly. It is the result of the momentum balance around the ejector which is shown in Fig. 12 together with the acting forces with their directions of action. The measured force

(6) $$F_{meas} = F_{FK} + F_{DK} - F_R - F_9$$

depends on the spring force F_{FK} of the expansion joint, the pressure force F_{DK}, the unknown friction force F_R and the gross thrust F_9. The spring force F_{FK} occurs due to an axial shift by Δs of the measurement slide. Δs is measured with displacement sensors. The pressure force F_{DK}, which acts on the expansion joint is generated by a pressure difference of the primary flow and the ambient pressure. Because the pipe on the left side of the expansion joint is mounted on a fixed-bearing the net thrust

(7) $$F_N = F_9 + F_5 = F_{FK} + F_{DK} - F_{meas} - F_R + F_5$$

is calculated by considering the inlet force F_5 of the primary flow. According to [21] F_5 can only be calculated with the measurement of pressure, temperature and mass flow in the core flow.

3.2.2. Measurement uncertainty

Measurement uncertainty is based on manufacturer specifications, standards and the evaluation according to GUM [23]. In Tab. 1 the remaining stochastic errors of all input quantities are listed. This is the source for the calculation of error propagation concerning the thrust augmentation factor.

Measure	2σ	Description
T_s, T_t	$\pm$ 0.4 K	Static and total temperatures
p_s, p_t	$\pm$ 0.05 %	Static and tot. pressures
A_{60}, A_9	$\pm$ 8 $\times$ 10^{-6} m^2	Nozzle areas
A_{ex}	$\pm$ 2 $\times$ 10^{-5} m^2	Exp. joint operative area
D_{ex}	$\pm$ 2 N mm^{-1}	Exp. joint spring rate
Δs	$\pm$ 3 $\times$ 10^{-7} m	Change in length
F	$\pm$ 0.5 N	Force (of the meas. range)
$\dot{m}_{60}$	$\pm$ 0.5 %	Primary mass flow

Tab. 1: Twice the standard deviation of single measurements.

For each operating point 600 individual measurements were carried out. The spread was identified by applying "root sum square" method and was added to the error in Tab. 1. The system showed a good repeatability. Dependent on $p_{t,60}/p_{t,0}$ and ε, thrust augmentation factor ϕ can be measured with an accuracy between 0.46 and 1.4 % as shown in Tab. 2. It is concluded that the achieved measurement uncertainty at higher pressure ratios is just good enough to measure the effects of interest.

	$\phi \pm 2\sigma$		
$p_{t,60}/p_{t,0}$	ε = 0.3	ε = 0.4	ε = 0.5
1.4	1.4 %	0.95 %	0.88 %
1.6	1.1 %	0.75 %	0.62 %
1.8	0.97 %	0.61 %	0.46 %

Tab. 2: Twice the standard deviation for the thrust augmentation factor ϕ [24].

3.2.3. Measurements

Thirty different geometrical combinations including five area ratios with $0.3 \leq \varepsilon \leq 0.5$ and six length ratios with $1.71 \leq \lambda \leq 6.59$ have been investigated. For each combination six nozzle pressure ratios $p_{t,60}/p_0$ between 1.6 and 1.9 were investigated.

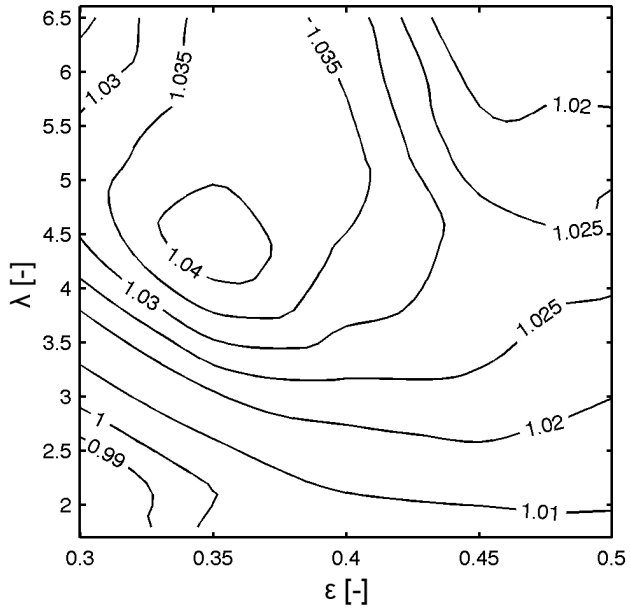

Fig. 13: Contours of thrust augmentation factor for a nozzle pressure ratio of 1.6.

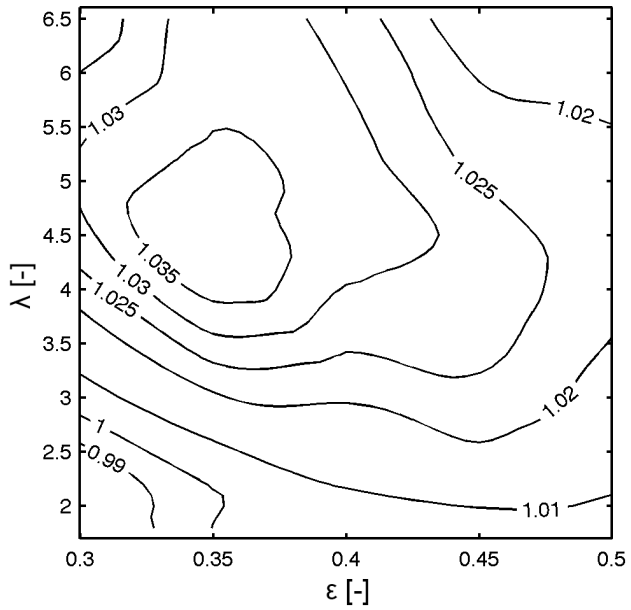

Fig. 14: Contours of thrust augmentation factor for a nozzle pressure ratio of 1.8.

In Fig. 13 and Fig. 14 thrust augmentation factor is shown as function of the geometric parameters for a nozzle pressure ratio of respectively 1.6 and 1.8 in the form of a contour plot.

The achieved thrust augmentation is at maximum less than or equal 4 % . Its optimum depends on the ejector geometry and was at about ε = 0.35 and λ = 4.5. A longer ejector resulted in a loss of thrust augmentation. According to [5] this is mainly because of the additional wall friction losses. More uneven velocity profiles at smaller values of λ indicate, that shorter ejectors lead to incomplete mixing and thus to a loss in thrust augmentation, see Fig. 15.

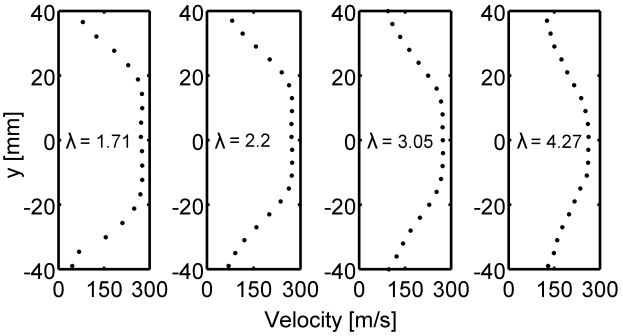

Fig. 15: Velocity profiles at ejector exit for ε = 0.4 and four different length ratios from λ = 1.71 to λ = 4.27. y is a coordinate along the ejector diameter.

Variation of area ratio ε alters the thrust augmentation. This results from the control volume analysis, as shown earlier in [25] [5]. Variation of nozzle pressure resulted in a slight change of thrust augmentation. Results for different nozzle pressure ratios varied within the range of measurement uncertainty of ϕ.

4. SUMMARY

Ejector nozzles featuring geometries typical for small jet engines have been investigated. Flow phenomena have been qualitatively visualized in a water channel. It was found that both mixing and pumping power are dependent on the geometric parameters λ, ε and the velocity parameter ζ. At the ejector test rig, ejector power was evaluated using the thrust augmentation parameter ϕ for geometrically different ejectors in various operating points. A maximum of 4% of thrust augmentation has been observed at values of $\varepsilon = 0.35$ and $\lambda = 4.5$.

5. AKNOWLEDGEMENT

The authors would like to express their gratitude to the State Graduate Sponsorship Program (Landesgraduiertenförderung) Baden-Württemberg for their financial support of this project.

REFERENCES

[1] NGUEWO, D.: *Erstellung und Optimierung der Skalierungsgesetze zur Abschätzung der Aerodynamik und der Eigendynamik eines Flugzeugs auf der Basis von frei fliegenden Modellen*. Ph.D. thesis, Universität Stuttgart, Institut für Flugzeugbau, 2007.

[2] KUPCIS, E.: The results of a low-speed wind tunnel test to investigate the effects of the Refan JT8D engine target thrust reverser on the stability and control characteristics of the Boeing 727-200 airplane. (1974).

[3] HUANG, B.; CHANG, J.; WANG, C.; PETRENKO, V.: A 1-D analysis of ejector performance. Tech. Rep. 354-364, 1998.

[4] CAMPBELL, W.; VON OHAIN, H.: Thrust Augmentation for V/STOL. Tech. Rep. ARL 67-0065, Energetics Research Laboratoy, 1967.

[5] PRESZ, W.; REYNOLDS, G.; HUNTER, C.: Thrust Augmentation with Mixer/Ejector Systems. *40th AIAA Aerospace Sciences Meeting and Exhibit*, (2002)(2002-0230).

[6] NAGARAJA, K.: Advances in Ejector Technology - A Tribute to Hans von Ohain's Vision. *Air Force Wright Aeronautical Laboratories Flight Dynamics Laboratory Wright-Patterson Air Force Base, Ohio*, (1982).

[7] ALPERIN, M.; WU, J.J.: Thrust augmenting ejectors, part I. *AIAA journal*, vol. 21 (1983)(10) pp. 1428–1436.

[8] ALPERIN, M.; WU, J.J.: Thrust augmenting ejectors, II. *AIAA journal*, vol. 21 (1983)(12) pp. 1698–1706.

[9] QUINN, B.: Ejector performance at high temperatures and pressures. *Journal of Aircraft*, vol. 13 (1976)(12) pp. 948–954.

[10] YANG, T.T.; NTONE, F.; JIANG, T.; PITTS, D.: An investigation of high performance, short thrust augmenting ejectors. *Journal of fluids engineering*, vol. 107 (1985)(1) pp. 23–30.

[11] PRESZ, W.M.; MORIN, B.K.L.; GOUSY, R.G.: Forced mixer lobes in ejector designs. *Journal of Propulsion and Power*, vol. 4 (1988)(4) pp. 350–355.

[12] HACKADAY, G.L.: Thrust Augmentation for a Small Turbojet Engine. Tech. rep., DTIC Document, 1999.

[13] RIEDEBERGER, D.: Design, Implementation and Evaluation of a Passive Thrust Augmentation Device for the SR-30 Turbojet. *Research paper, Institut of Aircraft Propulsion Systems (ILA), Stuttgart University*, (2010).

[14] BAUER, M.: *Modulares Leistungsberechnungsverfahren zur automatisierten modellbasierten Leistungsanalyse von Gasturbinen*. Ph.D. thesis, Institut für Luftfahrtantriebe der Universität Stuttgart, 2005.

[15] STREHBLOW, D.: *Experimentelle Untersuchungen am Wasserkanal zu Mischungsvorgängen in Ejektoren*. Research paper, Institut für Luftfahrtantriebe der Universität Stuttgart, 2013.

[16] BANZHAF, B.: *Untersuchungen zum Betriebsverhalten gemischter Abgassysteme in Luftstrahltriebwerken im niedrigen Lastbereich*. Ph.D. thesis, Institut für Luftfahrtantriebe der Universität Stuttgart, 2009.

[17] SABIN, C.M.: An analytical and experimental study of the plane, incompressible, turbulent free-shear layer with arbitrary velocity ratio and pressure gradient. *Journal of Basic Engineering*, vol. 87 (1965) p. 421.

[18] AHMED, M.; SHARMA, S.: Effect of velocity ratio on the turbulent mixing of confined, co-axial jets. *Experimental thermal and fluid science*, vol. 22 (2000)(1) pp. 19–33.

[19] JOUNBLAT, R.: *Visualisierung der Strömung von Ejektoren im Wasserkanal*. Research paper, Institut für Luftfahrtantriebe der Universität Stuttgart, 2013.

[20] GINEVSKI, A.: Theory of Turbulent Jets and Wakes in Russian. *Mashinostroenie, Moscow*, vol. 32 (1969).

[21] BOHL, W.; ELMENDORF, W.: *Technische Strömungslehre*. Vogel Verlag, 2005.

[22] REIZE, F.: *Planung, Konstruktion und Aufbau eines Ejektorprüfstandes zur Validierung des SAEPP Ejektormoduls und der numerischen Strömungssimulation*. Master's thesis, Institut für Luftfahrtantriebe der Universität Stuttgart, 2013.

[23] JOINT COMMITTEE FOR GUIDES IN METROLOGY: Evaluation of measurement data - An introduction to the 'Guide to the expression of uncertainty in measurement', Deutsche Fassung Auswertung von Messdaten - Eine Einführung zum 'Leitfaden zur Angabe der Unsicherheit beim Messen'. *BIPM*, (2009).

[24] RAMIN, S.: Erweiterung eines Ejektorprüfstands zur Bestimmung des Betriebsverhaltens eines geometrisch variablen Ejektors. *Research paper, Institut of Aircraft Propulsion Systems (ILA), Stuttgart University*, (2013).

[25] GEORGI, J.; STAUDACHER, S.; FALALEEV, S.: Modelling of an Ejector for Turbine Aeroengines for Application in Performance Synthesis Tools. In: *Vestnik, ISSN 1998-6629*, 3/(27). SSAU, Samara, 2011, pp. 337–344.